Universiteit Leiden
The Netherlands

Studies on Intracellular Logistics

Spits, M.

Citation
Spits, M. (2021, September 8). *Studies on Intracellular Logistics*. Retrieved from https://hdl.handle.net/1887/3209250

Version:	Publisher's Version
License:	Licence agreement concerning inclusion of doctoral thesis in the Institutional Repository of the University of Leiden
Downloaded from:	https://hdl.handle.net/1887/3209250

Note: To cite this publication please use the final published version (if applicable).

Cover Page

Universiteit Leiden

Leiden University Repository

The handle https://hdl.handle.net/1887/3209250 holds various files of this Leiden University dissertation.

Author: Spits, M.
Title: Studies on Intracellular Logistics
Issue Date: 2021-09-08

Chapter Two

HOMEOSTASIS OF SOLUBLE PROTEINS AND THE PROTEASOME POST NUCLEAR ENVELOPE REFORMATION IN MITOSIS

Menno Spits[1], Lennert J. Janssen[1], Lenard M. Voortman[1], Raymond Kooij[1], Anna C.M. Neefjes[1], Huib Ovaa[1] and Jacques Neefjes[1]

[1]Department of Cell and Chemical Biology, Oncode Institute, Leiden University Medical Center LUMC, Leiden NL

Journal of Cell Science. 2019 May 10.1242/jcs.225524

Abstract
Upon Nuclear envelope (NE) fragmentation in the prometaphase the nuclear and cytosolic proteomes blend and must be redefined to reinstate homeostasis. Using a molecular GFP ladder, we show that in early mitosis, condensed chromatin excludes cytosolic proteins. When the NE reforms tightly around condensed chromatin in late mitosis, large GFP multimers are automatically excluded from the nucleus. This can be circumvented by limiting DNA condensation with Q15, a Condensin II inhibitor. Soluble small and other NLS-targeted proteins then swiftly enter the expanding nuclear space. We then examined the proteasome, located in cytoplasm and nucleus. A significant fraction of 20S proteasomes is imported by importin IPO5 within 20 minutes following reformation of the nucleus, after which import comes to an abrupt halt. This suggests that maintaining the nuclear-cytosol distribution after mitosis requires chromatin condensation to exclude cytosolic material from the nuclear space and specialized machineries for nuclear import of large protein complexes such as the proteasome.

Introduction
Compartmentalization between the cytoplasm and nucleus is the defining characteristic of eukaryotic organisms, or those composed of 'true' cells. This separation in eukaryotic cells is afforded by the complex double-membrane structure of the nuclear envelope. Exchange of materials across this barrier occurs primarily through the nuclear pore complex (NPC), which allow passive diffusion of substances up to a size of roughly 70kDa, although recent work suggests that specific NPC qualities can infer some flexibility to this cut-off (Popken et al, 2015; Timney et al, 2016). Generally, molecules above that size cut-off are disallowed entry from the cytoplasm into the nucleus, unless they possess signal sequences, such as an nuclear localization signal (NLS), or bind to nuclear import carriers to specifically license active transport via the NPC(Chook & Suel, 2011; Goldfarb et al, 2004; Naim et al, 2007; Timney et al., 2016; Wang & Brattain, 2007). In addition to the inherited genome and other nucleic acids, nuclei contain a proteome distinct from that of the cytoplasm. All nuclear proteins are synthesized by cytosolic or ER-associated ribosomes and must subsequently cross the NE barrier to reach their site of action. The resulting compartmentalization allows separation of coupled processes in space and time to support optimal functioning of cells(Hung & Link, 2011; Stelma et al, 2016; Wang & Li, 2014).
In mammalian cells (and the majority of primitive Eukaryotes) the nucleoplasm/cytoplasm dichotomy is challenged at the onset of mitosis.

In prophase, when the NE fragments in preparation for chromosomal alignment and segregation, soluble nuclear and cytosolic proteins can suddenly occupy the same cellular space as the barrier between these compartments is lost. The question then is how the original localization of these two protein pools is restored once the NE reforms in cytokinesis with support of ESCRT-III and spastin(Guttinger et al, 2009; Olmos et al, 2015; Prunuske & Ullman, 2006; Vietri et al, 2015; Vietri et al, 2016). One option is that, while nuclear constituents benefit from NLS-dependent targeting, those proteins and complexes normally found in the cytosol, such as for instance the ribosome, could become erroneously captured by the nascent nuclear space and must then find a way out(David et al, 2012). This would then imply nuclear inclusion of the tRNA machinery and more, as required for full translation and it is likely that such mix-ups would be disfavoured. Whether and how this occurs, is studied here.

Results

Chromosomal condensation ensures exclusion of soluble cytosolic material from the newly formed nucleus post mitosis.

To visualize the fate of soluble proteins as a function of size, we constructed an incremental ladder of GFP multimers ranging from mono- to hexaGFP stably expressed in MelJuSo cells (**Fig. S1A**). Under steady state conditions, mono-, di- and triGFP filled both nuclear and cytosolic compartments, while penta- and hexaGFP were restricted to the cytosol (**Fig. 1A**). Quantification of fluorescence over the two compartments showed an equal distribution of mono-, di- and triGFP, as opposed to reduced nuclear distribution of tetraGFP and near complete nuclear exclusion of penta- and hexaGFP (**Fig. 1A**). These observations are consistent with the accepted notion that the NPC allows passive diffusion of proteins up to 50-70 kDa, but restricts larger cargoes unless they harbor an exposed NLS(Lange et al, 2007; Nigg, 1997), as illustrated by the predominantly nuclear localization of SV40 NLS-heptaGFP (**Fig. 1A**).

To follow the fate of cytosolic GFP during mitosis—and their return to the appropriate compartment of residence—we co-expressed mCherry-LaminA to visualize the timing of NE breakdown and reformation in conjunction with a DNA dye, SiR-DNA, to visualize the mitotic process. (Moriuchi et al, 2016). To simultaneously differentiate mitotic stages during time-lapse imaging, chromosomes were labeled with the far-red dye SiR-DNA. We first followed the distribution through mitosis of the GFP dimer that locates in both nucleus and cytoplasm during interphase (Fig. 1B, Video 1). We found that diGFP was excluded from

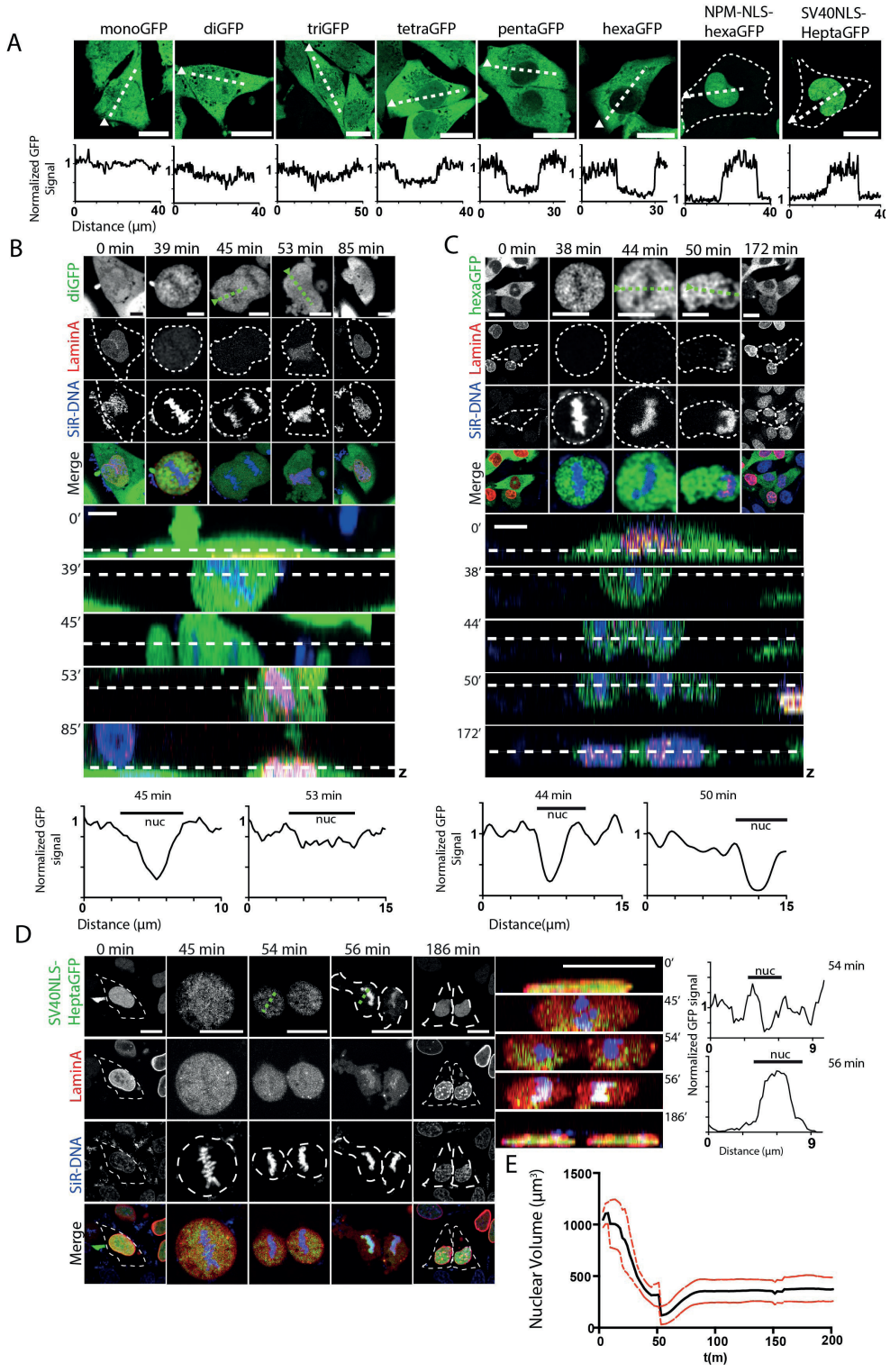
A
monoGFP
diGFP
triGFP
tetraGFP
pentaGFP
hexaGFP
NPM-NLS-hexaGFP
SV40NLS-HeptaGFP
Normalized GFP Signal
Distance (µm)
B
0 min
39 min
45 min
53 min
85 min
diGFP
LaminA
SiR-DNA
Merge
0′
39′
45′
53′
85′
z
45 min
53 min
nuc
Normalized GFP signal
Distance (µm)
C
0 min
38 min
44 min
50 min
172 min
hexaGFP
LaminA
SiR-DNA
Merge
0′
38′
44′
50′
172′
z
44 min
50 min
nuc
Normalized GFP Signal
Distance(µm)
D
0 min
45 min
54 min
56 min
186 min
SV40NLS-HeptaGFP
LaminA
SiR-DNA
Merge
0′
45′
54′
56′
186′
54 min
56 min
nuc
Normalized GFP signal
Distance (µm)
E
Nuclear Volume (µm³)
t(m)

Figure 1. Condensed chromatin as physical barrier for soluble proteins during mitosis.
(A) Confocal images of MelJuSo cells stably expressing the linear GFP multimers ranging from mono to hexaGFP (green) as well as hexaGFP with a nuclear localization signal and SV40 NLS-heptaGFP are shown. Corresponding pixel plot analyses depicting fluorescence intensities (normalized to the average) as measured along the dotted white lines are given below the images. Triangles denote the start of each line profile. Scale bars 20µm. (B,C) Select confocal z-slices and orthogonal slices from time-lapse experiments collected at 124 s intervals of MelJuSo cells stably expressing diGFP (B) or hexaGFP (C) (green) along with mCherry-LaminA (red) and stained with SiR-DNA (blue). At each timepoint, eight different z-stacks (as indicated in the side view in lower 5 panels) were made to define the location of chromatin. Data shown are representative of 4 independent acquisitions. Pixel plots of the green signal over the dotted green lines are shown below. Nuc shows the position of the nucleus, as marked by SiR-DNA. Scale bars, 20µm Related to Videos 1 and 3. (D) Select confocal z-slices and orthogonal slices from time-lapse experiments collected at 124 s intervals of MelJuSo cells stably expressing SV40 NLS-heptaGFP (green) along with mCherry-LaminA (red) and stained with SiR-DNA (blue). At each timepoint, eight different z-stacks (as indicated in the side view in 5 panels on the right) were made to define the location of chromatin. Stills correspond to Video 4. Images shown are representative of 3 acquisitions. Corresponding pixel plot analyses depicting fluorescence intensities (normalized to the average) as measured along dotted green lines are given below the images. Triangles denote the start of each line profile, nuc = the position of the nucleus, as marked by SiR-DNA. Scale bars, 20µm. (E) Volumetric analysis of cellular DNA (marked using SiR-DNA) as a function of time during representative time-lapse experiments of MelJuSo cells at different phases of mitosis. Graph displays the average (black line) and SD (red lines) of the nuclear volume in µm3 of 10 cells.

condensed chromosome density up to and including anaphase (t=45 min), similar as observed for microinjected fluorescent Dextran (Swanson & McNeil, 1987). However, 8 min later (t=53 min), coincident with the return of the DNA-associated LaminA signal, diGFP once again filled the nuclear as well as cytoplasmic space. The same pattern of behavior was observed for monoGFP (**Fig. S1B, Video 2**). To compare mitotic behavior of proteins below the NPC size cut-off with those above this threshold, we evaluated mitotic cells expressing hexaGFP (**Fig. 1C, Video 3**). Similar to its smaller counterparts, hexaGFP was excluded from the condensed DNA space during early mitosis. However, by contrast to diGFP (**Fig. 1B**), hexaGFP did not enter the expanding nascent nucleus after NE reformation (**Fig. 1C, t=50 min**). Since we visualized chromatin using SiR-DNA, we were also able to determine its volume across different phases of mitosis (**Fig. 1D**). This reveals that condensed chromatin during mitosis has a 3-fold smaller volume, which might explain the restricted space for small proteins to enter the condensed chromatin space. The sharp drop represents the actual chromosome division, which is then followed by an expansion of the DNA volume that will progress until it reaches a volume corresponding to the mother nucleus. These initial experiments reveal that soluble proteins belonging in the cytosol (small and large alike) are excluded from the space occupied by condensed chromosomes during most of mitosis. Then, in late mitosis, smaller proteins like the GFP dimer rapidly diffuse in the nuclear space following NE reformation (as timed by LaminA) concomitant with the expansion of nuclear

volume (**Fig. 1E**), similar as recently observed (Cai et al, 2018). Conversely, proteins larger than the limit of diffusion through the NPC remain excluded from the nuclear volume even as the nascent nucleus swells. Together, these observations suggest that cells have evolved a physical mechanism to avoid erroneous capturing of cytoplasmic materials inside the nuclei of newborn cells.If soluble cytosolic proteins are excluded from the nuclear space during mitosis, what is then the fate of soluble nuclear proteins? To address this, we fused hexaGFP to a bipartite nuclear localization sequence (NLS) of nucleoplasmin and heptaGFP to monopartite NLS of SV40 (Kalderon et al, 1984; Nigg, 1997) and followed the resulting NPM NLS-hexaGFP and SV40 NLS-heptaGFP through mitosis (**Fig. 1D and S2C; Video 4 and Video 5**). Strikingly, the presence of SV40 NLS enabled a small fraction of SV40 heptaGFP to blend with the condensed chromatin up to and during anaphase (t=54 min). Stably expressing SV40 NLS-heptaGFP cells clearly lack the exclusion conferred by chromosomal condensation. This suggests a closer proximity of heptaGFP to the condensed chromosomes now that its decorated with an NLS. Following NE reformation, the small portion of chromatin blended SV40 NLS-heptaGFP is likely encapsulated in the nascent nucleus (t=56 min), while the remaining cytosolic pool of SV40 NLS-heptaGFP was rapidly imported into the nucleus. Conversely, when studying NPM NLS-hexa-GFP, we observed slight enrichment of NPM NLS-hexaGFP on condensed chromosomal material. The NLS sequence apparently affects the interaction with chromatin components, as a variable fraction locates in the condensed chromatin space. Nevertheless, these observations suggest that unlike soluble cytoplasmic proteins, a small fraction of soluble nuclear proteins containing SV40 or NPM NLS are in close proximity of condensed chromatin during mitosis while the majority of NLS-hexaGFP or NLS-HeptaGFP locates outside the condensed chromatin space. When the nucleus reforms around condensed chromatin, it is followed by nuclear expansion(Lu et al, 2011) and these NLS-containing proteins then swiftly are imported in the nucleus.

Limiting chromosomal condensation by Q15 compromises soluble proteome homeostasis

To test whether nuclear exclusion of larger cytosolic proteins following NE reformation (as observed in **Fig. 1C**) requires the preceding exclusion of these materials as a result of chromosomal density, we aimed to limit chromatin condensation and then followed the fate of hexa-GFP that is excluded from the nucleus under unmanipulated situations. To this end, we synthesized a condensin inhibitor Anilinoquinazoline 15

(Q15) (Shiheido et al, 2012) that targets hGAP-G2 (a subunit of Condensin II) and thus limits chromosomal condensation (Hirano, 2005). Incubation of MelJuSo cells expressing hexaGFP in the presence of Q15 for 48 hrs yielded many dead cells, which is not unexpected when manipulating chromatin condensation. However, a significant number of cells that survived contained hexaGFP in the nucleus as opposed to the cells treated with DMSO (**Fig. A,C and D, video 5 and video 6**). Time-lapse microscopy of cells over mitosis suggests that, when compared to DMSO treated hexaGFP expressing cells, Q15 treatment locates a fraction of hexaGFP in the periphery of the chromatin in mitosis (**Fig. 2B**). Once decondensation commences, hexaGFP is allowed to diffuse in the decondensating chromatin space and is trapped in the newly formed nucleus. This assumes that Q15 does not permeabilize the NE. We treated stably expressing hexaGFP expressing cells with Q15 for 48 hr and bleached the nuclear hexaGFP signal. If Q15 would have permeabilized the nucleus, cytosolic hexaGFP would have restored fluorescence in the nucleus. However, no recovery of fluorescence was observed over a 30 minutes time period post bleaching (**Fig. 2E, video 8**). This further suggests that a physical parameter (the condensed state of chromatin during mitosis) is critical for protein homeostasis in nuclear and cytosolic compartments over mitosis.

The 20S proteasome requires a specialized mechanism for nuclear import post-mitosis

We then wondered how large protein complexes present in both compartments, such as the proteasome, are handled over cell division(Reits et al, 1997). The 20S proteasome—a protein complex of 750kD—should be far too large to swiftly diffuse across the NE. To test the dynamics of proteasome import in and export from the nucleus, we performed fluorescence recovery after photobleaching (FRAP) experiments to follow the kinetics of nuclear import of LMP2(Beta1i)-GFP-labeled proteasomes in MelJuSo cells. LMP2-GFP is stably incorporated into the 20S proteasome and no free LMP2 –GFP subunits have been detected (**Fig. 3A and B, Video 9**)(Reits et al., 1997). Following nuclear bleaching, recovery of nuclear GFP fluorescence from cytosolic proteasome entering the nucleus was not observed over a 10 min period. In fact, FRAP experiments did not reveal nuclear import of proteasomes even over a 3 hrs period (Reits et al., 1997). If proteasomes are excluded from the condensed chromatin space in accordance with observations for free soluble proteins, it would imply that newly formed nuclei are devoid of proteasomes for a considerable time period post-mitosis(Palmer et al, 1994; Savulescu et al, 2011). We therefore followed the fate of

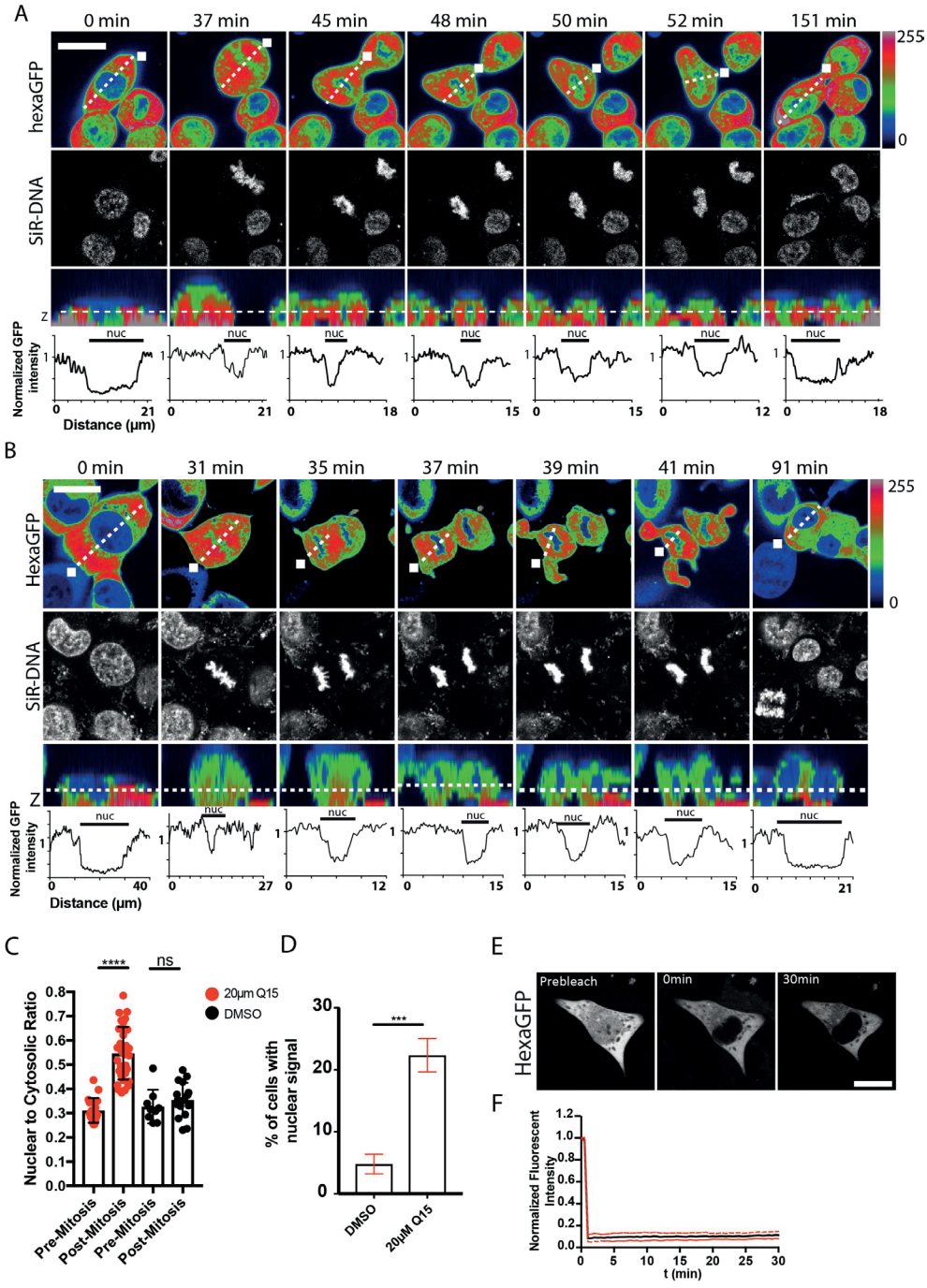

LMP2-GFP-labeled proteasomes over mitosis (**Fig. 3C, Video 10**). As in the case of GFP multimers, proteasomes were excluded from the con-

Figure 2. Soluble proteome dynamics disrupted during mitosis upon Q15 treatment. A,B Select confocal z-slices and orthogonal slices from time-lapse experiments collected at 124 s intervals of MelJuSo cells stably expressing hexaGFP (Green) and stained with SiR-DNA (Blue). The cells were treated with 20µM Q15 (A) or DMSO (B) for 48 hrs. At each timepoint, eight different z-stacks (as indicated in the side view in lower 5 panels) were made to define the location of chromatin. Data shown are representative of 3 independent acquisitions. Pixel plots of the GFP signal over the dotted white lines are shown below. White squares indicate the start of the measurement. Fluorescence intensities are represented in false colors according to the 'look-up' table in Fiji. Nuc shows the position of the nucleus, as marked by SiR-DNA. Stills correspond to Videos 6 and 7. Scale bars 20µm. (C) Quantification of nuclear to cytosolic ratio of 10 pre-mitotic cells and both their daughter cells from cells that A and B represent. Bars indicate mean + s.d. Statistical significance was calculated using Student's t test. ns, not significant, *** p>0,001, **** p<0,0001. (D) Quantification of cells (% of adherent population) harboring hexaGFP in the nucleus, 150 cells per experiment. Statistical significance was calculated using Student's t test. Bars indicate mean +/- s.d. from independent replicates. ***p<0,001. (E) Dynamics of the stably expressing hexaGFP cells. Cells were treated with 20µM Q15 for 48 hrs. Nuclei of cells harboring nuclear signal were bleached and followed over a 30 min time period. Stills correspond to Video 8. Scale bars, 20µm. (F) Quantification of hexaGFP fluorescence over time in the nuclear compartment after FRAP. Graph represents the normalized fluorescence of 3 acquisitions and the red dotted line indicates s.d.

densed chromatin space (t=50 min). Strikingly, coincident with cytokinesis, a substantial fraction of labeled proteasomes rapidly entered the newly formed nucleus demarcated by LaminA (t=56 min). Quantification of the LMP2-GFP signal indicated swift nuclear import for some 20min after nuclear reformation followed by an abrupt termination of nuclear import. This may coincide with formation of functional nuclear pore complexes and NE reconstruction (Lafarga et al, 2002). Interestingly, nuclear import by LMP2-GFP marked proteasomes after NE formation was even faster than that of diGFP, which enters the nucleus by free diffusion (**Fig. 3D, Video 1**). Furthermore, quantifying the nuclear signal of GFP and for NPM NLS-hexaGFP the cytosolic signal, we found that proteasomal nuclear import is slightly faster than that of NPM NLS-hexaGFP, which requires an active NLS-dependent import machinery (**Fig. 3E**). Of note, the fluorescence intensity of LMP2-GFP-labeled proteasome is 10-20% higher in the post-mitotic nuclei than before, likely as a result of a higher concentration present in the still expanding nucleus (see also **Fig. 1E**).

Importin-5 conducts the post mitotic nuclear import of the 20S proteasome.

These observations can only be explained by an active nuclear import mechanism for the proteasome operational only for some 20 minutes following NE reformation. This system is then critical for rapid delivery of proteasomes in the newly formed nucleus allowing normal propagation of proteasome dependent degradation of a plethora of nuclear substrates. Such a system is unknown. One option is that cells possess a pre-defined nuclear proteasome subset that then simply returns to its original location post-mitosis by conventional nuclear import.

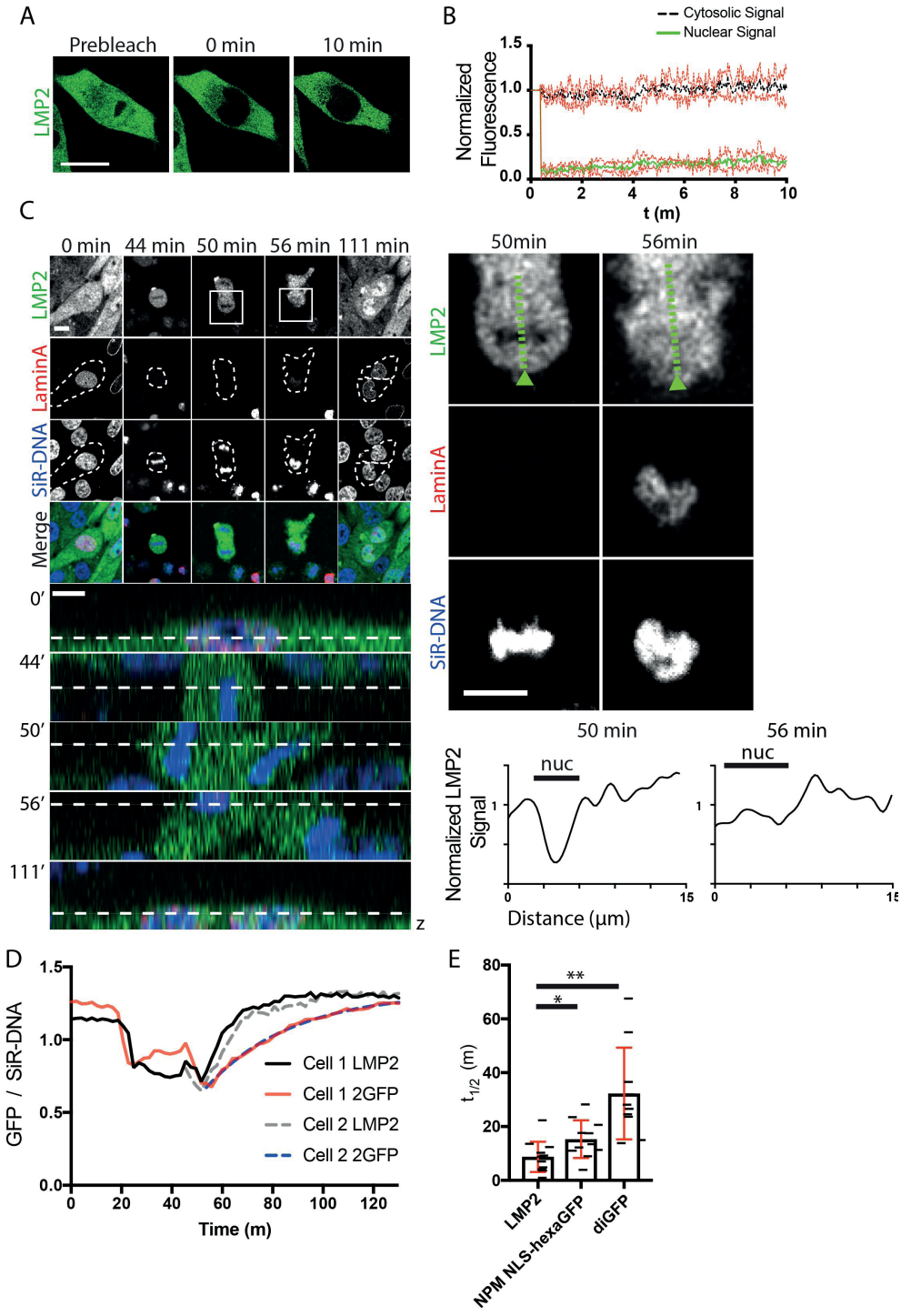
A
Prebleach
0 min
10 min
LMP2
B
Cytosolic Signal
Nuclear Signal
Normalized Fluorescence
t (m)
C
0 min
44 min
50 min
56 min
111 min
LMP2
LaminA
SiR-DNA
Merge
0′
44′
50′
56′
111′
z
50min
56min
50 min
56 min
nuc
Normalized LMP2 Signal
Distance (µm)
D
GFP / SiR-DNA
Time (m)
Cell 1 LMP2
Cell 1 2GFP
Cell 2 LMP2
Cell 2 2GFP
E
$t_{1/2}$ (m)
LMP2
NPM NLS-hexaGFP
diGFP

Figure 3. A wave of nuclear import of the 20S proteasome during mitosis
(A) Dynamics of the LMP2-GFP labelled proteasome. The nucleus of MelJuSo cells stably expressing LMP2-GFP was photobleached and the recovery of nuclear fluorescence was followed over a 10 min time period. Scale bar, 20µm. Stills correspond to Video 9. (B) Quantification of LMP2-GFP fluorescence with time in the nuclear and cytosolic compartments after FRAP. Graph represents the normalized fluorescence intensities of four acquisitions and the red dotted line indicates s.d. (C) Time-lapse confocal microscopy of MelJuSo cells stably expressing LMP2-GFP and co-expressing mCherry-LaminA. DNA was stained with SiR-DNA. Cells were followed for 16 hrs at 124 s intervals. At each timepoint, eight different z-stacks (as indicated in the side view in lower five panels) were made to define the location of chromatin. Scale bar, 20µm and for zoom-in (right panel), 10µm. Stills correspond to Video 10. Profile plots on the right represent normalized fluorescence intensities measured along the green dotted line of the corresponding image. The fluorescence intensities were normalized using the average fluorescence intensity of the measurement. The triangles denote the beginning of measurement of line profile plots. Nuc defines the location of the nucleus. (D) The ratio of normalized GFP intensities measured at location of SiR-DNA fluorescence in MelJuSo cells stably expressing diGFP, NLS-hexaGFP or LMP2-GFP through mitosis. The plot is a representative of 6 acquisitions for each condition. (E) Quantification of the half-time of nuclear import (t(1/2)) of GFP signal over SiR-DNA of MelJuSo cells stably expressing LMP2-GFP, NPM NLS-hexaGFP or diGFP through mitosis. Quantification was performed on 12 cells. Bars indicate mean + s.d. Statistical significance was calculated using Student's t test. ns, not significant, ** p>0,01, *** p<0,001.

To examine whether this is the case, we photobleached the nucleus of MelJuSo cells containing LMP2-GFP-labeled proteasomes and followed the remaining (cytosolic) fluorescence pool through mitosis **(Fig. 4A; Video 11**). While proteasomes were again excluded from condensed chromatin prior to cytokinesis (t=34 min), the original cytosolic pool of proteasomes now occupies both the cytosolic and nuclear compartments post-mitosis (**Fig. 4B**). This excludes the presence of a nucleus destined proteasome pool and implies a specialized mechanism active during a short phase late in mitosis and is responsible for the rapid targeting of proteasomes to newly formed nuclei. Another option would be that the proteasome dissociates in its free subunits that then diffuse in the nucleus to form a new proteasome. Since active proteasome subunits (including LMP2-GFP) contain a prosequence that is removed when the subunit is incorporated into the active proteasome, mature proteasome subunits would not be reincorporated into proteasomes (Jager et al, 1999; Li et al, 2016; Pante & Kann, 2002). In addition, we noted that the proteasome is entering the nucleus faster than diGFP that enters the nucleus by simple diffusion, again suggesting active nuclear import. In combination, these data propose a unique nuclear import system for the proteasome that is be active in a short time window immediately after NE formation.
Targeted nuclear import is driven by members of the karyopherin family(Chook & Suel, 2011; Goldfarb et al., 2004; Yang & Musser, 2006). Only a limited number of specific substrates have been defined for these importers, and none have thus far been described to mediate import of proteasomes to the nucleus in mammalian cells (Chook & Suel, 2011; Kimura et al, 2013; Pumroy & Cingola

ni, 2015; Stelma et al., 2016). It is likely that one or more karyopherins are involved in proteasome import after NE closure. To test this, we silenced importin expression using pools of small interfering RNAs (siRNA), followed by fixation and immunostaining for the endogenous proteasome. Comparison of nuclear to cytosolic fluorescence intensities identified Karyopherin A1 (KPNA1) and Importin-5 (IPO5) as candidates for nuclear proteasome import (**Fig. S2A**). We then deconvoluted the siRNA pools to confirm that silencing of IPO5 indeed reduced nuclear import of proteasomes in two different cell lines (**Fig. 4C Fig. S2B**). The efficiency of IPO5 depletion was validated by immunoblot (**Fig. 4D**). To assess whether expression of IPO5 would alter during mitosis, we determined IPO5 levels by Western blot, along with a marker (cyclin B1) that is degraded at a later phase of mitosis. Cells were synchronized, then released and samples were analyzed at the time points post-block release, as indicated (**Fig 4E**). No notable effect on IPO5 expression is detected, IPO5 may also alter its location in the short time window post-NE formation. We fixed and stained MelJuSo cells for IPO5 and LaminA/C and analyzed different phases in mitosis for their relative expression. In G0/G1 phase up to the late anaphase, IPO5 appears to localize primarily outside the nucleus. However, the nuclear localization of IPO5 increased as soon as LaminA/C appeared around the condensed chromatin (**Fig. 4G**) to return to a mainly cytosolic distribution shortly after this phase (for quantification, **Fig 4H**). These data suggest that IPO5 alters its activity during a short phase in mitosis and could then participate in the nuclear location of proteasomes Yet only a fraction of proteasomes are imported during this short phase. It is possible that IPO5 would be present in limiting amounts for more complete nuclear deposition of proteasomes. If so, IPO5 overexpression should increase the number of nuclear proteasomes. To test this, we ectopically expressed N-terminally GFP-tagged IPO5 in MelJuSo (**Fig. 4I and J**) and HeLa cells (**Fig. S2C and S2E**), followed by fixation and immunostaining for the 20S proteasome. We quantified the fluorescent signal and plotted the ratio between that in the nuclear and cytosolic compartments. Overexpression of IPO5, unlike another karyopherin family member KPNB1(Chook & Suel, 2011), indeed increased nuclear proteasome levels relative to the cytoplasm. To exclude that ectopic IPO5 expression would also accelerate nuclear import of proteasomes in G0/G1 phase, we performed FRAP experiments. We expressed mCherry-IPO5 in expressing LMP2-GFP cells and bleached GFP-proteasomes in the nucleus (**Fig. S2E, Video 11**). No recovery of signal in the two hours following bleaching was observed, implying that IPO5 overexpression does not accelerate nuclear import of (GFP-labelled) proteasomes in G0/G1 phase. Collectively, this iden

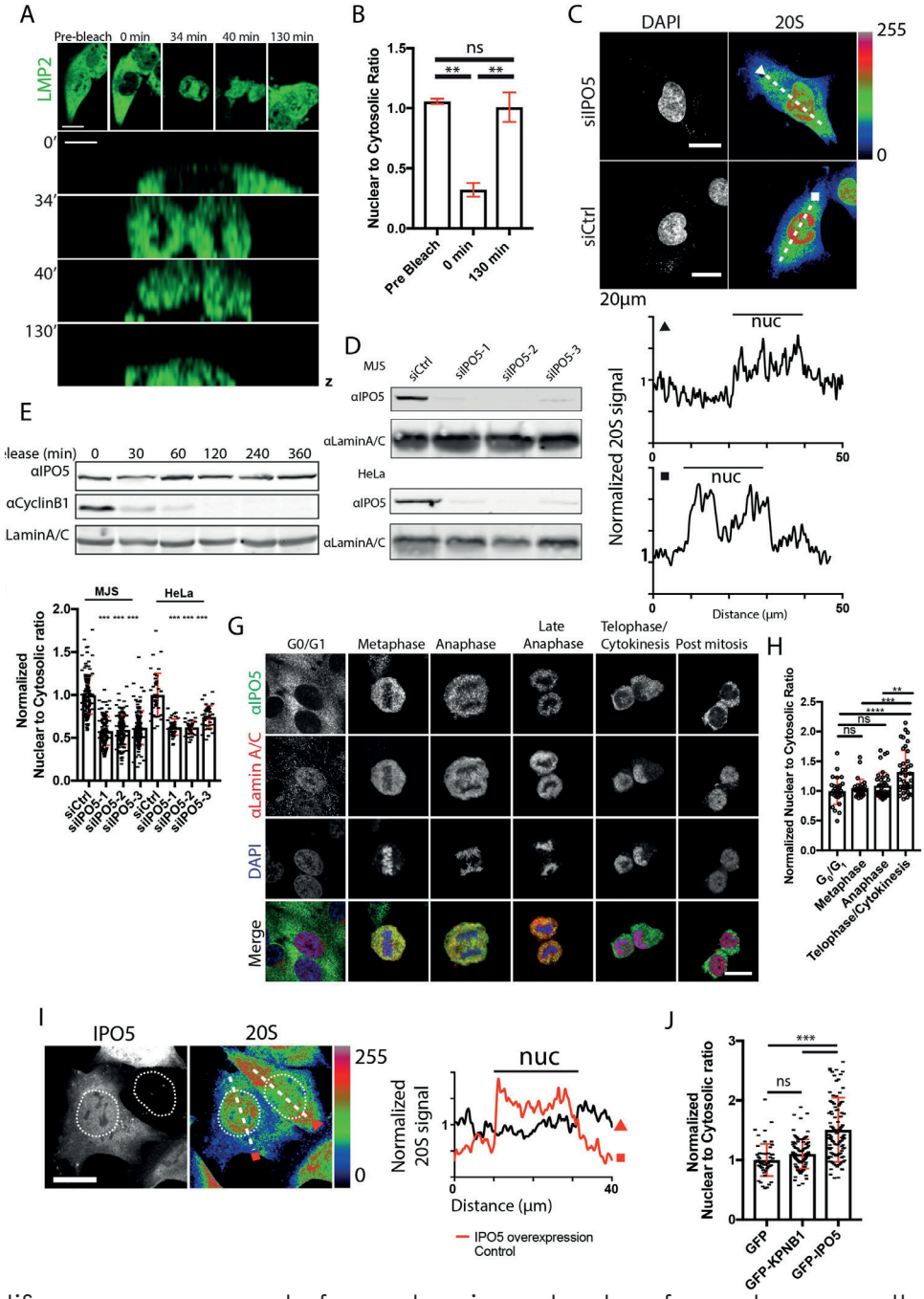

tifies one component of a nuclear import system for proteasomes that is active at a late phase in mitosis. This ensures rapid delivery of proteasomes excluded by condensed chromatin in the newly formed nucleus.

Figure 4. Importin-5 facilitates late mitotic nuclear import of 20S proteasomes.
(A) Time lapse confocal microscopy of MelJuSo cells expressing LMP2-GFP. The nuclear proteasomes were photobleached and cells imaged at 124s intervals. Side view in lower 4 panels from 8 z-stacks. Stills correspond to Video 11. Images are representative of two acquisitions. Scale bars, 20µm. (B) Quantification of the nuclear vs cytosolic fluorescence of cells from A. Bars show mean + s.d.; n=6 Bars indicate mean + s.d. Statistical significance was calculated using Student's t test. ns, not significant, ** p>0,01 (C) Confocal image of MelJuSo cells transfected with siRNA control or siRNA against IPO5. After 72 hrs, cells were fixed and stained for 20S proteasomes. DNA detected by DAPI staining. Fluorescence intensities are in false colors as indicated by the 'look-up' table. Profile plots on the right represent normalized fluorescence intensities measured along the white-dotted line. Nuc = the position of the nucleus marked by DAPI. See also Figure S2B Scale bar, 20µm. (D) Silencing efficiency in MelJuSo (MJS) and HeLa cells of IPO5 was determined by Western blot analysis for IPO5 and LaminA. (E) Western blot analysis of IPO5 levels in wild type MelJuSo cells during mitosis. MelJuSo cells were synchronized for 16 hrs with 75 ng/ml nocodazole. After a shake off to collect cells arrested in mitosis, cells were washed twice with PBS and reseeded. CyclinB1 served as an indicator for mitosis and LaminA/C as loading control. (F) MelJuSo and HeLa cells were transfected with siControl or individual siRNAs for IPO5. Cells were fixed and stained for 20S proteasomes. The nuclear/cytosolic ratio of fluorescence is depicted from 35 cells per siRNA condition, bars show mean+s.d. of three independent experiments. (G) Confocal images of wildtype MelJuSo cells. The cells were fixed and stained for IPO5, LaminA/C and DNA was stained with DAPI. Images represent two acquisitions. Scale bars, 20µm. (H) Quantification of nuclear to cytosolic ratio of endogenous IPO5 in several phases of the cell cycle from cells from G. The nuclear/cytosolic ratio of fluorescence is depicted from 15 cells per phase per replicate, bars show mean+s.d. of 2 replicates. (I) MelJuSo cells were transfected with GFP-IPO5 and stained for 20S proteasomes. The fluorescence intensities are shown in false colors. Right profile plot represents normalized fluorescence intensities measured along the white-dotted line. The fluorescence intensities were normalized using the average fluorescence intensity of the measurement. Nuc= position of the nucleus. Scale bar, 20µm. (J) Quantification of nuclear/cytosolic ratio of 20S proteasomes in cells ectopically expressing GFP, GFP-KPNB1 or GFP-IPO5. 30 cells per experiment were quantified, bars show mean+s.d. of three independent replicates, intensities were normalized using the average intensity of GFP. Statistical significance calculated using Student's t test. ns, not significant; *p>0,05; **P<0,01; ***P<0,001

Discussion

We have visualized a largely ignored aspect of mitosis: the restoration of the cytosolic and nuclear proteomes after NE reformation. Given the conserved nature of nuclear/cytoplasmic compartmentalization across species, its fidelity must be critical to the progeny's success. With commencement of mitosis, fragmentation of the NE eliminates the barrier between the nucleus and cytosol, resulting in a mixed soluble proteome. Our data provide a simple explanation for how cells repartition soluble proteins destined for either their cytosolic or nuclear compartments. We suggest that soluble proteins are generally excluded from the condensed chromatin space in mitosis. These data are in line with recent findings suggesting that small nuclear pores are present in the reforming NE starting from anaphase onset. The NPC pre-pores would allow free diffusion of cytosolic material if condensed DNA would not act as a physical barrier(Otsuka et al, 2018). A fraction of proteins are decorated with an NLS. We tested hexaGFP with two different NLS sequences, that had poor to low affinity for chromatin or nuclear import factors recognizing these signals. However, the majority of NLS-containing pro

teins is in the cytosolic volume immediately after the NE is reformed and is imported into the nucleus when nuclear expansion begins. We propose a simple model describing the maintenance of the nuclear and cytosolic proteomes during the cell cycle After nuclear disintegration, disintegration, the soluble nuclear and cytosolic proteome mixes. The chromatin is condensed to a density that excludes even small proteins such as GFP. Around the condensed chromatin the nuclear envelop is formed then physically excluding cytosolic proteins from the nuclear space. The nucleus will then start expanding to its original volume. Proteins with an NLS are at the same time rapidly re-imported from the cytosol in the nucleus and homeostasis of the soluble proteome is restored.

In this study we used the proteasome as an example of a macromolecule that exists in both cellular compartments. During mitosis the proteasome is also excluded from condensed chromatin and must be reimported into the nucleus to provide the machinery for protein turnover to new cells. Since nuclear import of the proteasome is slow (Reits et al., 1997), either new cells first live without nuclear proteasomes or another system for nuclear import of the proteasomes should exist. The NE is tightly sealed immediately after NE formation as illustrated by the effective exclusion of hexaGFP from the nuclear space. Proteasomes are much larger and should then also be excluded from the nucleus, at least through passive diffusion. It is also possible that a fraction of proteasomes are predestined for the nucleus. The 20S proteasome has been suggested to possess a NLS, but whether that is responsible for nuclear import of proteasomes is unclear(Knuehl et al, 1996; Nederlof et al, 1995; Ogiso et al, 2002).Yet, FRAP experiments exclude a specific nuclear pool of proteasomes. Instead, we observe a rapid and short import of proteasomes into the nuclear space after NE formation. The import is faster than free diffusion of diGFP which suggests that this should be an active system that is operational for only some 20 min post-NE formation. This is followed by a considerably slower nuclear import event of proteasomes. We show that at least one component of the large karyopherin family, IPO5, supports nuclear proteasome import. Despite extensive attempts, we failed to identify factors specifically marking proteasomes for IPO5-mediated nuclear import due to the difficulty of 'catching' factors active only 20 min post-NE formation. Yeast studies to nuclear import of proteasomes identified N-acetylation by SIRT family members as a factor controlling this process (van Deventer et al, 2015). Yeast does not fragment its nucleus during division and we do not know whether this modification is also relevant in nuclear import of proteasomes immediately after NE formation. N-acetylation may then affect multiple substrates including IPO5.

Which –if any- of these substrates may be critical in mammalian cells, is unclear. IPO5 has been implicated in nuclear import of beta-catenin (Goto et al, 2013), MSI1 (Sutherland et al, 2015), CBEP3(Chao et al, 2012) and influenza polymerase subunit PB1(Hutchinson et al, 2011), and these proteins are likely delivered to the nucleus in response to specific signals or infection. Because we excluded a dedicated nuclear proteasome fraction, dedicated biochemical events involving either the proteasome, IPO5 or other proteins should be operational during the first and final stages of mitosis that would drive the proteasome in the nucleus during some 20 min after NE formation. IPO5 is likely rate limiting in this process but not necessarily directly interacting with the proteasome. However, it is likely that additional factors will be involved in the nuclear import of the proteasome. Of note, the proteasome may be representative of other nuclear complexes, including possibly the spliceosome, RNA polymerases, or other large protein complexes without obvious NLS, that reside and function in the nucleus. This new biology has to be developed. We visualized an unexplored but critical aspect of the cell biology of mitosis that may be manipulated in order to control the life of mitotic cells. The nuclear exclusion of large cytosolic proteins after mitosis is the result of a physical process, the condensed state of mitotic chromatin that excludes these molecules. As the NE forms around the condensed chromatin before expansion, such cytoplasmic proteins are automatically excluded from the nuclear space. Proteins with an NLS will be located in the cytosol after NE formation and then swiftly imported back into the nucleus. The proteasome as a prototype large protein complex without clear NLS then requires specific import processes including IPO5 for nuclear import. This process is operational during a short period late in mitosis. Multiple processes then control protein complex homeostasis over mitosis in cells.

Materials and Methods

Cell Culture and Constructs

MelJuSo cells were cultured in IMDB (ThermoFischer Scientific, USA) supplemented with 10% FCS and HeLa cells in DMEM (ThermoFischer Scientific, USA) with 10% FCS. All cells were tested regularly for mycoplasma contamination and checked for contamination by other cells through morphological analysis. MelJuSo cells stably expressing LMP2 –GFP were previously described(Reits et al., 1997). A MelJuSo cell line was used to generate the stably expressing cell lines with constructs for monoGFP, diGFP, triGFP, tetraGFP, pentaGFP hexaGFP, NPM NLS-hexaGFP and SV40 NLS-heptaGFP. A cryptic start site in GFP as was the start methionine

was removed in the following GFP multimer using the following primers: 5'- CCCAAGATCTCTTGTACAGCTCGTCCAT-3', 5'-CCCAGGATCCGTGAGCAAGGGCGAGGAG-3' and 5'-CCCAGAATTCTCACTTGTA CCCAGAATTCTCACTTGTACAGCTCGTCCATGC-3'. These were cloned into a C1-mGFP vector using BglII, BamHI and EcoRI restriction, respectively. This was accomplished by generating a GFP without a start and stop codon and cloning it behind a wild type GFP lacking a stop codon. This was continued until hexaGFP was reached. For NLS-hexaGFP, an NLS sequence from Nucleoplasmin and from SV40 was cloned at the N terminus of the heptaGFP coding sequence using the following primers: for NPM 5'- CTAGCCACCATGGTGAAACGACCAGCAGCAACAAAGAAAGCAGGACAAGCAAAGAAAAAGAAGA-3' and 5'-CTAGTCTTCTTTTTCTTTGCTTGTCCTGCTTTCTTTGTTGCTGCTGGTCGTTTCACCATGGTGG-3' into C1 6GFP vector using NheI and SpeI restriction sites and for 2xSV40 5'-CTAGGCCACCATGCCAAAAAAAAAAAGTTA-3' and 5'-CTAGTAACTTTTCTTTTTTTTTTTGGCATGGTCG-3' into C1 6GFP vector using NheI, this was repeated to obtain 2xSV40 NLS. pBABE-puro-GFP-wt-LaminA was a kind gift from Tom Misteli(Scaffidi & Misteli, 2008) (Addgene plasmid # 17662) and cloned into a C1-mCherry expression vector using primers 5'-CCCAAGATCTATGGAGACCCCGTCCCAGC-3' and 5'-CCCAGAATTCGCGGCCGCTTACATGATGCTGCAGTTCT-3'. IPO5 was cloned from the ORFeome collaboration library cssbBroadEn_10938 using the primers 5'-CCCACTCGAGCCATGGCGGCGGCCGCG-3' and 5'-CCCAGGTACCTCACGCAGAGTTCAGGAGCTCCTGAAT-3' into mGFP-C1 and mCherry-C1 Vector with XhoI and Asp718I restriction sites. KPNB1 was cloned from IMAGE 3352610 using the primers 5'-CCCAGAGCTCCCATGGAGCTGATCACCATTCT-3' and 5'- CCCAGGATCCTCAAGCTTGGTTCTTCAGTTT-3' into mGFP-C1 vector using SacI and BamHI restriction sites. Shrimp Alkaline Phosphatase (ANZA, Thermofisher, USA) was used in cloning SV40-NLS-hexaGFP. All constructs were sequence verified.

Reagents and antibodies

Anilinoquinazoline 15 was synthesized as previously described and used at a concentration of 20μM for 48 hours(Shiheido et al., 2012). Nocodazole at a concentration of 75ng/ml was used to synchronize MelJuSo cells (Cayman Chemicals, USA). For live cell DNA staining, sirDNA 700 was added to cells ±20 min before the start of imaging (Spirochrome, Switzerland). For detection of human 20S proteasome by microscopy we used rabbit anti-20S (Enzo, USA) at a dilution of 1:100. This antibody recognizes many proteasomal subunits (beta5/beta7, beta1, beta5, beta5i and beta7). For Western blot analysis of GFP we

used rabbit anti-GFP at a dilution of 1:1000 (Rocha et al, 2009).Importin-5 (Karyopherin beta3) was detected by Western blot analyses using mouse anti-human IPO5 at a dilution of 1:1000 (Santa Cruz, USA). Rabbit anti-human Lamin A/C, at a dilution of 1:1000 (Santa Cruz, USA) was used for staining a loading control. Mouse anti-CyclinB1, at a dilution of 1:1000, was used to determine mitotic phase (Santa Cruz, USA). Secondary antibodies for microscopy were goat anti-mouse Alexa-488 goat, anti-rabbit Alexa-568 and anti-mouse Alexa-568 at a dilution of 1:400 (Life Technologies, USA). For detection of the primary antibodies by Western blot, goat anti-mouse 800CW IRDye, (1:10.000) and goat anti-rabbit 680RD IRDye (1:10.000) (Li-COR, USA) were used.

Transfection

For ectopic expression, MelJuSo and HeLa cells were transfected using Effectene (Qiagen, Germany) according to the manufacturer's instructions. For siRNA-mediated silencing, cells were reverse transfected with DharmaFECT transfection reagent #1 (Dharmacon, USA) and 50nM siRNA. Three days later the cells were fixed, stained and analyzed by confocal microscopy or Western blot. siRNAs for the screen were extracted from a human siGENOME siRNA library genome smart pool (Dharmacon, USA). For further studies, we used siRNA for IPO5 under code MQ-017318-02-0005 (Dharmacon, USA).

Western blotting

For whole cell lysate analyses, cells were lysed directly in SDS-sample buffer (2% SDS, 10% glycerol, 100mM DTT, 60mM Tris-HCl pH 6.8 and 0.01% bromophenol blue) and boiled for 10 minutes. Proteins were subsequently separated by SDS-PAGE and transferred to a nitrocellulose membrane (GE Healthcare, The United Kingdom). Blocking of the membrane was done in PBS supplemented with 5% (w/v) skim milk powder (OXOID, Netherlands). The membranes were imaged using the Odyssey Imaging System Clx (Li-COR, USA). Original Western blot images are presented in figure S3.

Confocal microscopy

Cells were seeded on coverslips and transfected. 18 hrs later, cells were fixed in 3,7% formaldehyde for 20 min and permeabilized in 0.01% Triton X-100 (Fisher Chemicals, USA) for 15 min. Staining was performed with the antibodies described above. The cell nuclei were stained with DAPI and the cells were mounted onto coverslips with prolong-gold anti-fade reagent with DAPI (Invitrogen, USA). Images were acquired using either a Leica TCS SP5 confocal microscope, a Leica TCS SP8 (Leica Microsys

tems, Wetzlar, Germany) at x63 magnification or an Andor Dragonfly 505 spinning disk confocal on a Leica DMi8 microscope (Oxford Instruments, United Kingdom). For live cell imaging, the microscopes wereequipped with a humidified climate control system at 37˚C supplemented with 5% CO2. All sequential images were collected at a rate of 124 seconds per frame for a period of 16 hrs. Time-lapse images were segmented using semi-automates procedures in ImageJ and Matlab (Mathworks, USA). Subsequent quantification was performed in Matlab by measuring the mean fluorescent intensity. To quantify the import half-time, we fitted an exponential function to the intensity data using the curve fitting toolbox of Matlab. All Images were processed using Adobe Illustrator and ImageJ.

Statistical analysis and experimental setup

All experiments shown in the paper were performed independently at least two times. For nuclear to cytosolic ratios numerical values were calculated and subsequently normalized using either siControl treated samples or cells expressing GFP. Statistical significance was calculated using an unpaired student t test. Statistical values are as following *P<0.05, **p<0.01, ***p<0,001, ****p<0.0001.

Online supplemental material

Figure 1S shows a Western blot analysis of cells stably expressing the molecular GFP ladder and stills representing Video 2 and NPM NLS-hexaGFP stills corresponding to video 5. Figure 2S shows confocal microscopy images MelJuSo cells treated with the siRNA screen and its quantification and similar images from HeLa cells overexpressing IPO5 and the quantification of HeLa cells overexpressing IPO5, KPNB1 or GFP as well as confocal data and the quantification of MelJuSo cells stably expressing LMP2-GFP and overexpressing mCherry-IPO5 subjected to FRAP experiment. Figure S3 shows the uncropped Western blot analysis of figure 4D and 4E.

Acknowledgements

We thank the microscopy facilities of the NKI and the LUMC for their support and members of the Neefjes group for critical discussions.

Competing Interests

The authors declare no competing interests

Author contributions

MS performed all cell biological experiments. This work followed a

question of the then 16 year-old ACMN to her high schoolteacher, who did not know the answer. LJJ and MS generated the different DNA constructs. LMV and MS performed the image analyses. RK synthesized Q15. under the supervision of HO. This study was coordinated by JN.

Funding

This work was supported by an NWO TOP grant and an ERC Advanced Grant awarded to J.N. J.N. and H.O. are members of the Oncode Institute

References

Cai Y, Hossain MJ, Heriche JK, Politi AZ, Walther N, Koch B, Wachsmuth M, Nijmeijer B, Kueblbeck M, Martinic-Kavur M et al (2018) Experimental and computational framework for a dynamic protein atlas of human cell division. Nature 561: 411-415

Chao HW, Lai YT, Lu YL, Lin CL, Mai W, Huang YS (2012) NMDAR signaling facilitates the IPO5-mediated nuclear import of CPEB3. Nucleic Acids Res 40: 8484-8498

Chook YM, Suel KE (2011) Nuclear import by karyopherin-betas: recognition and inhibition. Biochim Biophys Acta 1813: 1593-1606

David A, Dolan BP, Hickman HD, Knowlton JJ, Clavarino G, Pierre P, Bennink JR, Yewdell JW (2012) Nuclear translation visualized by ribosome-bound nascent chain puromycylation. J Cell Biol 197: 45-57

Goldfarb DS, Corbett AH, Mason DA, Harreman MT, Adam SA (2004) Importin alpha: a multipurpose nuclear-transport receptor. Trends Cell Biol 14: 505-514

Goto T, Sato A, Adachi S, Iemura S, Natsume T, Shibuya H (2013) IQGAP1 protein regulates nuclear localization of beta-catenin via importin-beta5 protein in Wnt signaling. J Biol Chem 288: 36351-36360

Guttinger S, Laurell E, Kutay U (2009) Orchestrating nuclear envelope disassembly and reassembly during mitosis. Nat Rev Mol Cell Biol 10: 178-191

Hirano T (2005) Condensins: organizing and segregating the genome. Curr Biol 15: R265-275

Hung MC, Link W (2011) Protein localization in disease and therapy. J Cell Sci 124: 3381-3392

Hutchinson EC, Orr OE, Man Liu S, Engelhardt OG, Fodor E (2011) Characterization of the interaction between the influenza A virus polymerase subunit PB1 and the host nuclear import factor Ran-binding protein 5. J Gen Virol 92: 1859-1869

Jager S, Groll M, Huber R, Wolf DH, Heinemeyer W (1999) Proteasome beta-type subunits: unequal roles of propeptides in core particle maturation and a hierarchy of active site function. J Mol Biol 291: 997-1013

Kalderon D, Roberts BL, Richardson WD, Smith AE (1984) A short amino acid sequence able to specify nuclear location. Cell 39: 499-509

Kimura M, Okumura N, Kose S, Takao T, Imamoto N (2013) Identification of cargo proteins specific for importin-beta with importin-alpha applying a stable isotope labeling by amino acids in cell culture (SILAC)-based in vitro transport system. J Biol Chem 288: 24540-24549

Knuehl C, Seelig A, Brecht B, Henklein P, Kloetzel PM (1996) Functional analysis of eukaryotic 20S proteasome nuclear localization signal. Exp Cell Res 225: 67-74

Lafarga M, Fernandez R, Mayo I, Berciano MT, Castano JG (2002) Proteasome dynamics during cell cycle in rat Schwann cells. Glia 38: 313-328

Lange A, Mills RE, Lange CJ, Stewart M, Devine SE, Corbett AH (2007) Classical nuclear localization signals: definition, function, and interaction with importin alpha. J Biol Chem 282: 5101-5105

Li X, Li Y, Arendt CS, Hochstrasser M (2016) Distinct Elements in the Proteasomal beta5 Subunit Propeptide Required for Autocatalytic Processing and Proteasome Assembly. J Biol Chem 291: 1991-2003

Lu L, Ladinsky MS, Kirchhausen T (2011) Formation of the postmitotic nuclear envelope from extended ER cisternae precedes nuclear pore assembly. J Cell Biol 194: 425-440

Moriuchi T, Kuroda M, Kusumoto F, Osumi T, Hirose F (2016) Lamin A reassembly at the end of

mitosis is regulated by its SUMO-interacting motif. Exp Cell Res 342: 83-94
Naim B, Brumfeld V, Kapon R, Kiss V, Nevo R, Reich Z (2007) Passive and facilitated transport in nuclear pore complexes is largely uncoupled. J Biol Chem 282: 3881-3888 Nederlof PM, Wang HR, Baumeister W (1995) Nuclear localization signals of human and Thermoplasma proteasomal alpha subunits are functional in vitro. Proc Natl Acad Sci U S A 92: 12060-12064
Nigg EA (1997) Nucleocytoplasmic transport: signals, mechanisms and regulation. Nature 386: 779-787
Ogiso Y, Tomida A, Tsuruo T (2002) Nuclear localization of proteasomes participates in stress-inducible resistance of solid tumor cells to topoisomerase II-directed drugs. Cancer Res 62: 5008-5012
Olmos Y, Hodgson L, Mantell J, Verkade P, Carlton JG (2015) ESCRT-III controls nuclear envelope reformation. Nature 522: 236-239
Otsuka S, Steyer AM, Schorb M, Heriche JK, Hossain MJ, Sethi S, Kueblbeck M, Schwab Y, Beck M, Ellenberg J (2018) Postmitotic nuclear pore assembly proceeds by radial dilation of small membrane openings. Nat Struct Mol Biol 25: 21-28
Palmer A, Mason GG, Paramio JM, Knecht E, Rivett AJ (1994) Changes in proteasome localization during the cell cycle. Eur J Cell Biol 64: 163-175
Pante N, Kann M (2002) Nuclear pore complex is able to transport macromolecules with diameters of about 39 nm. Mol Biol Cell 13: 425-434
Popken P, Ghavami A, Onck PR, Poolman B, Veenhoff LM (2015) Size-dependent leak of soluble and membrane proteins through the yeast nuclear pore complex. Mol Biol Cell 26: 1386-1394
Prunuske AJ, Ullman KS (2006) The nuclear envelope: form and reformation. Curr Opin Cell Biol 18: 108-116
Pumroy RA, Cingolani G (2015) Diversification of importin-alpha isoforms in cellular trafficking and disease states. Biochem J 466: 13-28
Reits EA, Benham AM, Plougastel B, Neefjes J, Trowsdale J (1997) Dynamics of proteasome distribution in living cells. EMBO J 16: 6087-6094
Rocha N, Kuijl C, van der Kant R, Janssen L, Houben D, Janssen H, Zwart W, Neefjes J (2009) Cholesterol sensor ORP1L contacts the ER protein VAP to control Rab7-RILP-p150 Glued and late endosome positioning. J Cell Biol 185: 1209-1225
Savulescu AF, Rotem A, Harel A (2011) Proteasomes crossing the nuclear border. Nucleus 2: 258-263
Scaffidi P, Misteli T (2008) Lamin A-dependent misregulation of adult stem cells associated with accelerated ageing. Nat Cell Biol 10: 452-459
Shiheido H, Naito Y, Kimura H, Genma H, Takashima H, Tokunaga M, Ono T, Hirano T, Du W, Yamada T et al (2012) An anilinoquinazoline derivative inhibits tumor growth through interaction with hCAP-G2, a subunit of condensin II. PLoS One 7: e44889
Stelma T, Chi A, van der Watt PJ, Verrico A, Lavia P, Leaner VD (2016) Targeting nuclear transporters in cancer: Diagnostic, prognostic and therapeutic potential. IUBMB Life 68: 268-280
Sutherland JM, Sobinoff AP, Fraser BA, Redgrove KA, Davidson TL, Siddall NA, Koopman P, Hime GR, McLaughlin EA (2015) RNA binding protein Musashi-1 directly targets Msi2 and Erh during early testis germ cell development and interacts with IPO5 upon translocation to the nucleus. FASEB J 29: 2759-2768
Swanson JA, McNeil PL (1987) Nuclear reassembly excludes large macromolecules. Science 238: 548-550
Timney BL, Raveh B, Mironska R, Trivedi JM, Kim SJ, Russel D, Wente SR, Sali A, Rout MP (2016) Simple rules for passive diffusion through the nuclear pore complex. J Cell Biol 215: 57-76
van Deventer S, Menendez-Benito V, van Leeuwen F, Neefjes J (2015) N-terminal acetylation and replicative age affect proteasome localization and cell fitness during aging. J Cell Sci 128: 109-117
Vietri M, Schink KO, Campsteijn C, Wegner CS, Schultz SW, Christ L, Thoresen SB, Brech A, Raiborg C, Sten mark H (2015) Spastin and ESCRT-III coordinate mitotic spindle disassembly and nuclear envelope sealing. Nature 522: 231-235
Vietri M, Stenmark H, Campsteijn C (2016) Closing a gap in the nuclear envelope. Curr Opin Cell Biol 40: 90-97
Wang R, Brattain MG (2007) The maximal size of protein to diffuse through the nuclear pore is larger than 60kDa. FEBS Lett 581: 3164-3170
Wang X, Li S (2014) Protein mislocalization: mechanisms, functions and clinical applications in cancer. Biochim Biophys Acta 1846: 13-25

Yang W, Musser SM (2006) Nuclear import time and transport efficiency depend on importin beta concentration. J Cell Biol 174: 951-961

Supplemental data

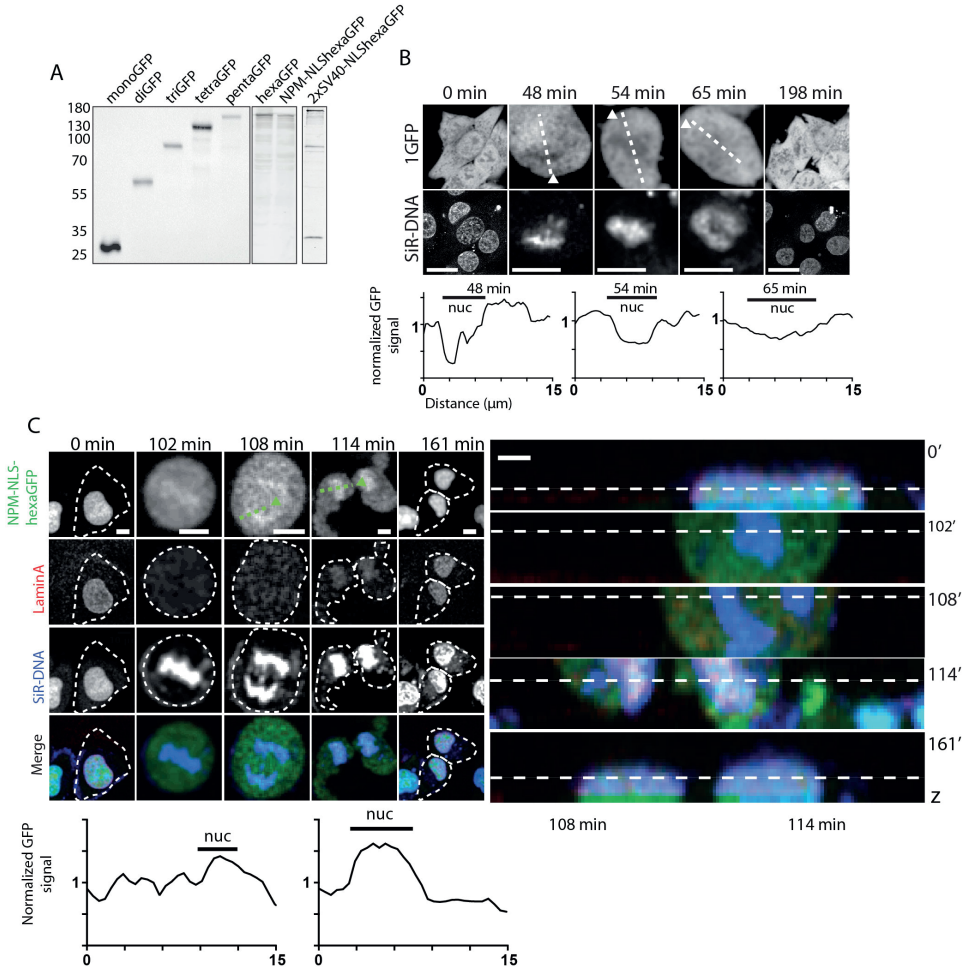

Figure S1. Western blot analysis of GFP multimers and tagged proteins and their nuclear and cytosolic compartmentalization

(A) MelJuSo cells stably expressing mono to hexaGFP or NLS-hexaGFP were lysed an analyzed by SDS-PAGE and Western blotting for GFP. The position of the marker proteins is indicated. (B) Time lapse confocal microscopy of MelJuSo cells stably expressing monoGFP. DNA was stained with SiR-DNA. The cells were imaged for 16 hrs at 125 s intervals. Different z-stacks were made to define the location of chromatin. Stills correspond to supplemental video 2. The images are representative of four acquisitions. Profile plots below represent normalized fluorescent intensities measured along the line of the cell above. The fluorescent intensities were normalized using the average fluorescence intensities of the measurement. Nuc= the position of the nucleus, as marked by SiR-DNA. Scale bars 20µm

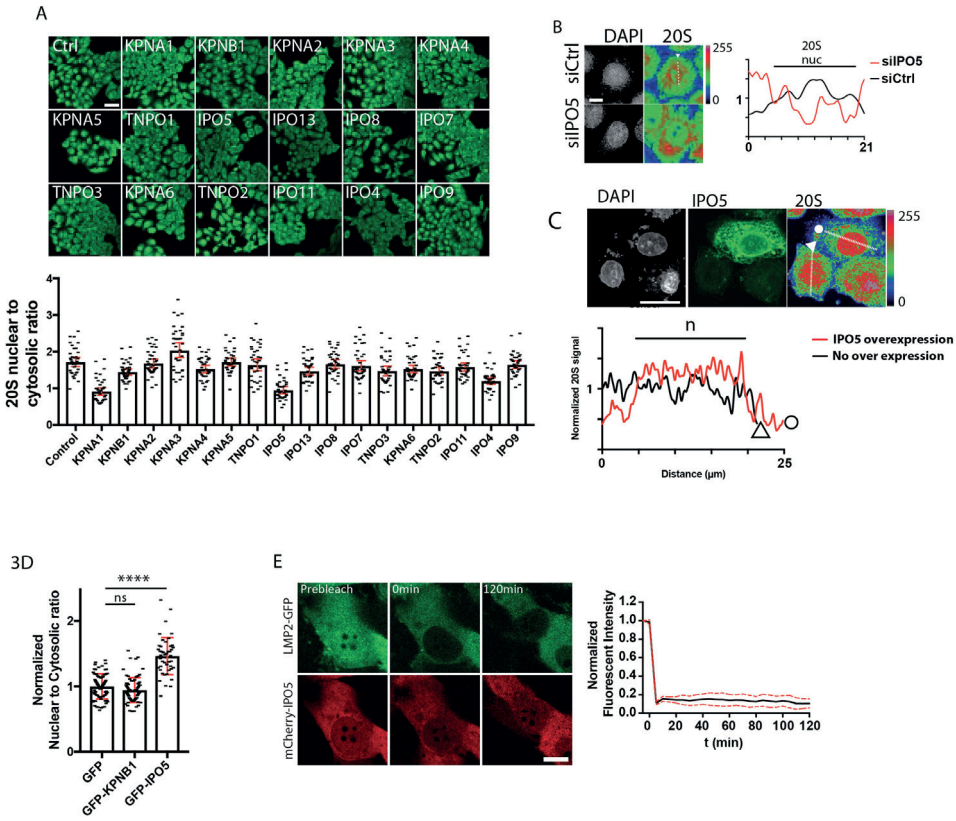

Figure S2. Karyopherin-alpha and Karyopherin-beta siRNA screen reveals IPO5 and KPNA1 as potential candidates for proteasome import and the effect of silencing or overexpression on nuclear localization of the 20S proteasome

(A) Fields of MelJuSo cells transfected with siControl or an siRNA of a panel directed against Karyopherin-alpha and Karyopherin-beta family members, as indicated. The cells were stained for 20S proteasome. Scale bar 50µm. (B) HeLa cells were transfected with siControl or one of three siIPO5 constructs.16 hrs post-transfection, cells were stained for 20S proteasome. The fluorescent intensities are shown in false colors as indicated by the 'look-up' table in Fiji. Profile plots on the right represent normalized fluorescent intensities measured along the line of the corresponding image. The fluorescent intensities were normalized using the fluorescent signal intensity of the measurement. Scale bar 20µm. (C) HeLa cells were transfected with GFP, GFP-IPO5, or GFP-KPNB1 and fixed and stained for 20S proteasome 16 hrs post-transfection. The fluorescent intensities are shown in false colors as indicated by the 'look-up' table in Fiji. Profile plots on the right represent normalized fluorescent intensities measured along the line of the corresponding image. The fluorescent intensities were normalized using the average fluorescent intensity of the measurement. Nuc shows the position of the nucleus, as marked by DAPI. Scale bar 20µm (D) Quantification of nuclear to cytosolic ratio of 20S proteasome fluorescence of cells from C, >30 cells per experiment were quantified, bars show mean + s.d. of two independent replicates, intensities were normalized using the average intensity of GFP. Ns, not significant, ****P<0,0001

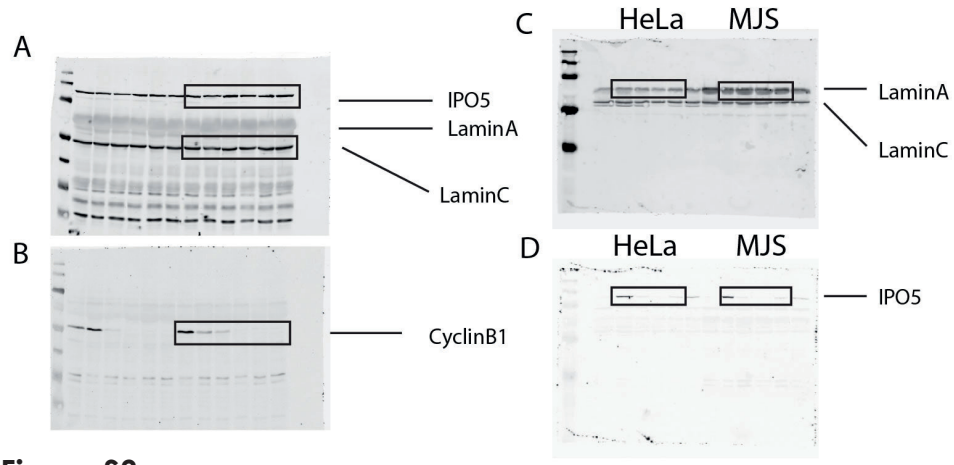

Figure S3
Uncropped Western blot scans from figure 4F

Video 1
Time-lapse images corresponding to stills of figure 1B

Video 2
Time-lapse images corresponding to stills of supplemental figure 2

Video 3
Time-lapse images corresponding to stills of figure 1C

Video 4
Time-lapse images corresponding to stills of figure 2A

Video 5
Time-lapse images corresponding to stills of figure 3A

Video 6
Time-lapse images corresponding to stills of figure 3C

Video 7
Time-lapse images corresponding to stills in figure 4A